A RESEARCH ON E-NVH PERFORMANCE COMPREHENSIVE OPTIMIZATION OF IPMSM FOR EV BASED ON NSGA-Ⅲ

Sili Ma[1], Quanfeng Li[2]*

[1]*Shanghai DianJi University, Shanghai, China*
[2]*Shanghai DianJi University, Shanghai, China*
**liqf@sdju.edu.cn*

Keywords: ELECTRIC VEHICLES, IPMSM, AUXILIARY SLOT, MULTI-OBJECTIVE OPTIMIZATION

Abstract

Electromagnetic performance, noise, vibration and harshness (E-NVH) are very important considerations in the design of interior permanent magnet synchronous motor (IPMSM) for electric vehicles (EV). To promote the E-NVH performance of IPMSM, a novel multi-objective optimization methodology incorporating rotor auxiliary slots for targeted suppression of harmonic electromagnetic forces (EMF) is proposed in this paper. The dominant space-time harmonic orders of EMF that demonstrate significant suppression effects on E-NVH performance are identified theoretically. The Pareto-optimal solution for auxiliary slot geometry parameters is derived through a parametric optimization methodology utilizing the third-generation nondominated sorting genetic algorithm (NSGA-III). As validated through finite element analysis (FEA) simulations, the optimized IPMSM configuration demonstrates a 45.14% improvement in E-NVH performance compared to the prototype.

1 Introduction

E-NVH performance is considered a critical indicator for assessing the quality and market competitiveness of EV. IPMSM have been widely adopted in EV due to their superior power factor and efficiency [1]. However, unlike internal combustion engine vehicles, EV rely solely on electric motor propulsion [2]. The absence of internal combustion engine masking effects exacerbates E-NVH challenges in IPMSM, particularly with respect to electromagnetic-induced acoustic resonances [3]. Driven by the escalating consumer demand for premium ride comfort functionalities, E-NVH performance optimization has garnered intensified research focus in both academic and industrial domains [4]. The vibro-acoustic generated by IPMSM are classified into three categories based on their excitation mechanisms [5]: electromagnetic vibro-acoustic, aerodynamic vibro-acoustic, and mechanical vibro-acoustic [6]. Among these, electromagnetic vibration constitutes the predominant contributor to E-NVH, primarily induced by harmonic EMF that exert excitation on stator teeth, thereby inducing structural deformation and subsequent mechanical vibration [7]. The electromagnetic vibration characteristics of IPMSM are intrinsically linked to the spatiotemporal harmonic content of EMF, with zeroth-order radial force waves playing a dominant role in vibrational response mechanisms [8]. Research indicates that zeroth-order vibration excited by modulation effects of high-order force harmonics in integer-slot IPMSM poses a primary challenge to E-NVH performance [9]. A phase compensation methodology integrating vibro-inertance theory and operational force measurement enables precise identification of dominant excitation sources under Multiphysics coupling conditions[10]. Regarding vibration mitigation strategies, the directional rotor step-skewing technique disrupts the phase continuity of force waves, resulting in a significant reduction of the modulated vibration[11]. The incorporation of auxiliary slots on the rotor surface serves to suppress specific harmonic orders in the air-gap flux density, thereby reducing torque pulsations and electromagnetic vibrations in electric machines [12]. Nevertheless, the identification of spatiotemporal harmonic orders in electromagnetic excitation forces and their targeted suppression remain a critical research gap in E-NVH performance optimization for EV traction motors.

Current research on E-NVH performance optimization for electric machines predominantly focuses on electromagnetic metrics such as cogging torque and torque ripple as optimization targets, with no existing literature addressing E-NVH as a holistic performance objective. Moreover, the majority of existing studies employ second-generation genetic algorithms for multi-objective optimization. In contrast, third-generation genetic algorithms exhibit superior capabilities in handling high-dimensional objectives, generating more uniformly distributed nondominated solution sets, while demonstrating enhanced convergence properties and computational efficiency. In this paper, a novel multi-objective optimization method based on the rotor auxiliary slot targeting to weaken the harmonic EMF is proposed to improve the E-NVH performance of an 8-pole 48-slot IPMSM. Based on the third-generation non-dominated sequential genetic algorithm (NSGA-III) with the size and position parameters of the auxiliary slots as the optimization variables, a comprehensive optimization study is carried out with the objectives of reducing the harmonic EMF density and torque pulsation of the target order and improving the average torque and efficiency.

2. Analysis of Magnetic Fields and Dominant Radial EMF

According to motor theory, when an IPMSM is powered by sinusoidal current, the magnetic potential in its air gap can be decomposed into three main components: the fundamental wave magnetic potential generated by the stator windings, the harmonic magnetic potential of the stator windings, and the harmonic magnetic potential of the rotor permanent magnets. As in equation (1):

$$\begin{cases} f_p(\theta,t) = F_p \cos(p\theta - \omega_0 t - \varphi_0) \\ \sum_{\nu} f_\nu(\theta,t) = \sum_{\nu} F_\nu \cos(\nu\theta - \omega_0 t - \varphi_1) \\ \sum_{\mu} f_\mu(\theta,t) = \sum_{\mu} F_\mu \cos(\mu\theta - \mu\omega_0 t / p - \varphi_2) \end{cases} \tag{1}$$

Where F_p is the amplitude of the fundamental magnetic potential, P is the pole pair number, ω_0 is the angular frequency of the fundamental, φ_0 is the initial phase angle of the fundamental, F_ν is the amplitude of the νth harmonic magnetic potential, φ_1 is the initial phase angle of the νth harmonic. F_μ is the amplitude of the μth harmonic magnetomotive force and φ_2 is the initial phase angle of the μth harmonic. Thus, the air-gap magnetic potential of a permanent magnet synchronous motor can be expressed in equation (2):

$$f(\theta,t) = f_0(\theta,t) + \sum_{\nu} f_\nu(\theta,t) + \sum_{\mu} f_\mu(\theta,t) \tag{2}$$

The air-gap permeability is equation (3):

$$\begin{cases} \Lambda(\theta,t) = \Lambda_0 + \sum \lambda_{11} \\ \Lambda_0 = \dfrac{\mu_0}{k_\delta \delta} \\ \lambda_{11} = \Lambda_{l1} \cos(l_1 Z_1 \theta) \\ \Lambda_{l1} = \dfrac{\mu_0 (k_\delta - 1)}{k_\delta \delta} \left| \dfrac{\sin\left(l_1 \dfrac{k_\delta - 1}{k_\delta} \pi \right)}{l_1 \dfrac{k_\delta - 1}{k_\delta} \pi} \right| \end{cases} \tag{3}$$

Where Λ_0 is the invariant portion of air gap permeability per unit area, λ_{11} is the harmonic ratio permeability of the stator slotting caused by the periodic component of the permeability, μ_0 is the vacuum permeability, k_δ is the air gap coefficient, δ is the length of the air gap, and Z_1 is the number of stator slots. When the core reluctance is neglected, the air gap magnetism can be expressed as the product of the air gap magnetomotive potential and the air gap permeability. As in equation (4):

$$b(\theta,t) = f(\theta,t)\Lambda(\theta,t) \tag{4}$$

Bringing (2) and (3) into (4) yields an expression for the air gap magnetic field of a permanent magnet synchronous motor when powered by a sine wave, as in equation (5):

$$\begin{aligned} b(\theta,t) &= f(\theta,t)\Lambda(\theta,t) \\ &= F_0\Lambda_0 \cos(p\theta - \omega_0 t - \varphi_0) + \\ &\sum F_\nu \Lambda_0 \cos(\nu\theta - \omega_0 t - \varphi_1) + \\ &\sum F_\mu \Lambda_0 \cos(\mu\theta - \mu\omega_0 t / p - \varphi_2) + \\ &\sum \frac{F_0 \Lambda_{l1}}{2} \cos\left[(p \pm l_1 Z_1)\theta - \omega_0 t - \varphi_3 \right] + \\ &\sum\sum \frac{F_\nu \Lambda_{l1}}{2} \cos\left[(\nu \pm l_1 Z_1)\theta - \omega_0 t - \varphi_4 \right] + \\ &\sum\sum \frac{F_\mu \Lambda_{l1}}{2} \cos\left[(\mu \pm l_1 Z_1)\theta - \mu\omega_0 t / p - \varphi_5 \right] \end{aligned} \tag{5}$$

For integer slot motors, the number of stator-rotor harmonics is given by equation (6):

$$\begin{cases} \nu = (6k_1 + 1)p \\ \nu_t = \left(k_2 \dfrac{Z_1}{p} + 1 \right) p = k_2 Z_1 + p \\ \mu = (2k_3 + 1)p \end{cases} \tag{6}$$

ν is the number of stator harmonics, ν_t is the number of tooth harmonics, μ is the number of rotor harmonics, k_1, k_2, k_3 are all integers. The magnitude of electromagnetic vibration caused by radial EMF is related to two factors. One is the amplitude of the radial EMF, and the other is the spatial order of the radial EMF r. The deformation of the motor core during vibration is inversely proportional to r^4. A smaller spatial order results in greater deformation of the motor core. After removing the radial EMF of larger order and smaller amplitude, the expression for the radial EMF of the PMSM with sinusoidal supply is equation (7):

$$\begin{aligned} p_r = \frac{1}{2\mu_0} \Bigg\{ & \frac{B_0^2}{2} \cos(2p\theta - 2\omega_0 t - 2\varphi_0) + \\ & \sum_{\nu}\sum_{\mu}\sum_{l_1} B_\nu B_\mu \cos\left[(\mu \pm \nu \pm l_1 Z_1)\theta - (\mu / p \pm 1)\omega_0 t - \varphi_{14} \right] \Bigg\} \end{aligned} \tag{7}$$

Where B_0 is the fundamental amplitude of the air gap magnetization, B_ν and B_μ are the ν and μ harmonic amplitudes of the air gap magnetization. The spatial order r and temporal order of the radial EMF are calculated as equation (8):

$$\begin{cases} r = \mu \pm \nu \\ r_t = (2k_3 + 1 \pm 1)p \\ r_{\min} = \mathrm{GCD}(Z_1 / m, 2p) \end{cases} \tag{8}$$

r is the EMF space order, r_t is the EMF time order, $r_{\min}$ is the lowest non-zero space order of EMF, GCD is the computed greatest common divisor, and is the number of phases. For a motor with 8 poles and 48 slots, the lowest non-zero order of radial EMF space is 8. The lowest non-zero spatial order and the corresponding temporal order of the partial radial EMF to this motor are calculated using equation (8), as shown in Table1.

Table 1. Main spatial and temporal orders of radial EMF in an 8-pole, 48-slot IPMSM

Rotor harmonic \ Stator harmonic	4	-20	28	-44	52
4	0/0				
12	8/8	-8/16			
20		0/24	-8/16		
28		8/32	0/24		
36			8/32	-8/40	
44				0/48	-8/40
52				8/56	0-48

From (6), the stator first-order tooth harmonic orders for the 8-pole, 48-slot are -44 and 52. Therefore, for the 8-pole, 48-slot PM synchronous motor, special attention needs to be paid to the radial spatial EMFs of time orders 24 and 48 for spatial order 0.

3 Verification by FEA and Optimization by Algorithm Design

The magnetic field of an 8-pole/48-slot motor is analyzed by the analytical method in Chapter 2, and the temporal and spatial orders of the main EMF contributing to the vibration are determined. In order to verify the correctness of the analytical method analysis, the finite-element simulation analysis of radial EMF and algorithmic optimization and design of IPMSM are carried out in this chapter.

The 2D finite element model of this 8-pole/48-slot IPMSM is shown in Fig. 1. Firstly, the air-gap magnetic density data of the motor under rated operating conditions are obtained by simulation, and then the radial EMF of IPMSM is calculated using Eq. (7) with the spatial and temporal distributions as shown in Fig. 2, and finally, the radial EMF is subjected to a two-dimensional Fourier decomposition in order to obtain the radial EMF density amplitude at each spatial and temporal order, as shown in Fig. 3.

The radial EMF of each time order under the rated working condition of the motor in space 0 order is shown in Table 2. It can be seen from the table that the radial EMF density of time 24 and 48 orders under space 0 order is larger, which is consistent with the theoretical analysis. In this paper, the radial EMF of space 0 order, time 24 and 48 order under rated conditions is taken as the optimization objective to optimize the design of IPMSM.

Rotor surface slotting is a method of reducing motor torque ripple and electromagnetic vibrations by attenuating specific order harmonics in the air gap magnetization. Since the airgap permeability is no longer equally distributed after the stator is slotted, the airgap magnetization is distorted, thus allowing the airgap magnetization waveform to contain higher order harmonics. By cutting auxiliary slots on the rotor surface, the sinusoidal of the air gap density can be optimized and the tooth harmonic content can be weakened. Four auxiliary slots are symmetrically opened on the rotor with the centreline of

Table 2. Radial EMF density for each time order at space order 0^{th}

Time order	Radial EMF density/N/m^2	Time order	Radial EMF density/N/m^2
0	259046.7	40	90.5
8	117.6	48	17818.9
16	199.9	56	314.0
24	14199.2	64	353.1
32	675.8	72	4384.8

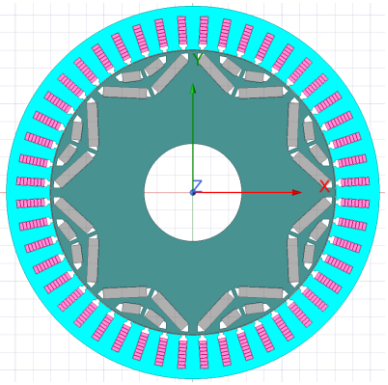

Fig. 1 IPMSM 2D finite element model

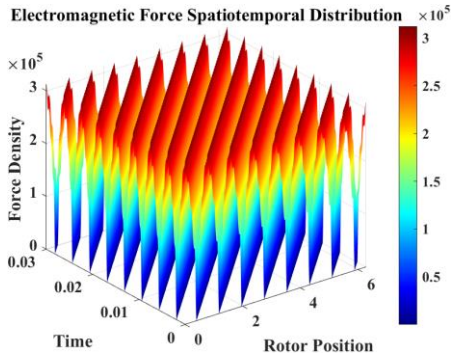

Fig. 2 Spatial and temporal distribution of EMF

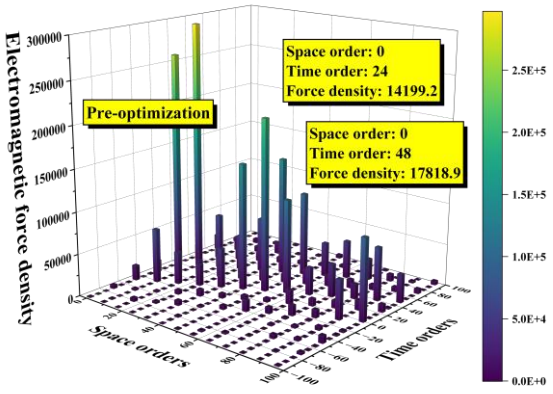

Fig. 3 Time-space order distribution of EMF

the magnetic poles, and the dimensions and positions of auxiliary slots No. 1,4 and No. 2,3 are symmetrical about the centreline of the magnetic poles, as shown in Fig. 4. The inner

Table 3. E-NVH sub-indicator weight setting

Parameter Types	Weight setting
EMF of space-0th/time-48th	0.5
EMF of space-0th/time-24th	0.2
Average torque	0.05
Torque ripple	0.2
Efficiency	0.05

Table 4. Parameter setting of NSGA-III

Parameter Types	Parameter value
Population size	50
Minimum population size	40
Number of iterations	30
Crossover coefficient	0.1
Variation coefficient	0.005

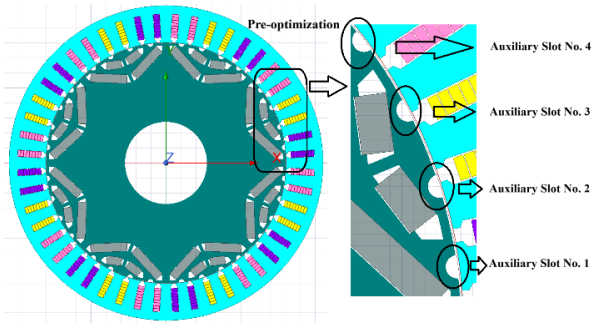

Fig. 4 Rotor auxiliary slots schematic

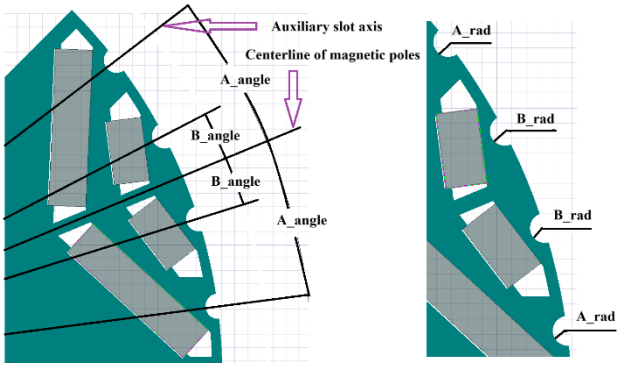

Fig. 5 Auxiliary slot size and position parameter schematic

diameters of the auxiliary slots No. 1 and No. 4 are indicated by A_rad; the angle between the axis where the centre of the circle is located and the centreline of the magnetic poles is indicated by A_angle, and the inner diameters of the auxiliary slots No. 2 and No. 3 are indicated by B_rad; and the angle between the axis where the center of the circle is located and the centreline of the magnetic poles is indicated by B_rad. The angle between the axis where the center of the circle is located and the centreline of the magnetic pole is expressed by B_angle, as shown in Fig. 5. The size and position of the auxiliary slot can be changed by changing the values of A_rad, B_rad, A_angle and B_angle.

Table 5. Optimize variable parameter settings

Optimization parameters	Initial value	Range of values	Optimized value
A_angle	15	12~20	14.7
B_angle	5	2~8	5.83
A_rad	1	0.5~1.5	1.5
B_rad	1	0.5~1.5	0.9

According to the analysis of EMF in Chapter 2, it is known that the order of radial EMF of 8-pole 48-slot motor which has a large impact on electromagnetic vibration noise is space 0 order time 24 order and space 0 order time 48 order, so they are selected as the direct optimization target of multi-objective optimization. In order that slotting does not have too much influence on the torque performance of the motor, the average torque and torque pulsation of the motor are taken as constraints to ensure that the torque performance of the motor meets the requirements. Thus the problem of multi-objective optimization can be described as (9):

$$\begin{aligned} &\min F_{r0\_24} \\ &\min F_{r0\_48} \\ &T_{\text{avg}} \geq 294\text{N}\cdot\text{m} \\ &T_{\text{rip}} \leq 15\% \end{aligned} \tag{9}$$

Where $F_{r0\text{-}24}$ is the spatial 0th order time 24th order radial EMF, $F_{r0\text{-}48}$ is the spatial 0th order time 48th order radial EMF, T_{avg} is the average torque, and T_{rip} is the torque pulsation. In order to evaluate the optimization effect of the comprehensive performance of E-NVH more intuitively, weights are set for the optimization effects of sub-indicators, i.e., the target order harmonic electromagnetic force density, torque pulsation, average torque, and efficiency, and it is defined that the optimization effect of the E-NVH index is equal to the optimization effect of the sub-indicators multiplied by the corresponding weights and then added up. The detailed settings of the weights are shown in Table 3.

In the field of multi-objective optimization of electric machines, the main advantages of the third generation of genetic algorithms over the second generation are that they can handle multiple objectives more efficiently and generate a more uniformly distributed set of non-dominated solutions, as well as having better convergence and computational efficiency. In this paper, multi-objective optimization is performed based on NSGA-III with the position and size of the auxiliary slot on the rotor surface as variables, and the spatial 0th order time 24th order and 48th order EMF as objectives. The parameter settings regarding NSGA-Ⅲ are shown in Table 4.

The multi-objective optimization results are shown in Fig. 6, the above shows all the optimization schemes and the optimal set of solutions. Where the optimal solution is selected based on the pareto front surface optimized by the third generation genetic algorithm. The optimal auxiliary slot parameters are further verified by evaluating the average torque, torque pulsation, and efficiency. The range of values of the

optimization variables and the optimized values are shown in Table 5.

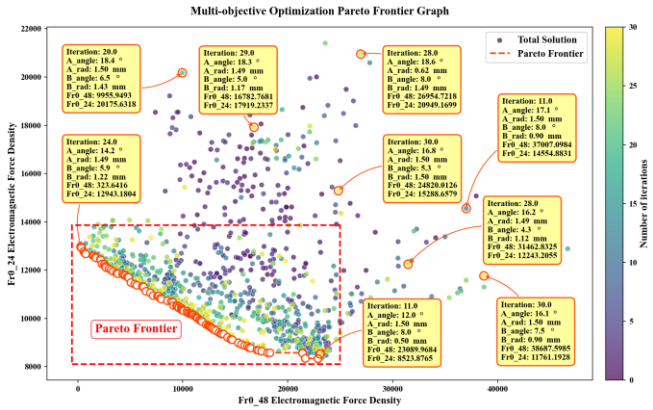

Fig. 6 Multi-objective optimization pareto frontier graph

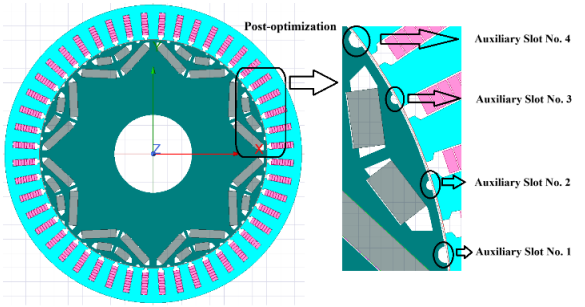

Fig. 7 Optimized motor model

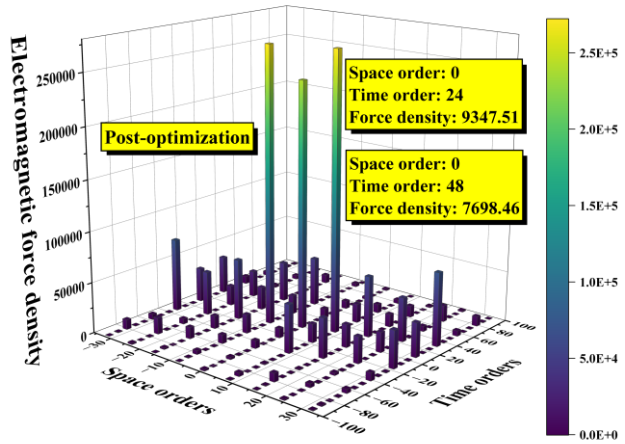

Fig. 8 Spatial-temporal order of the optimized EMF

According to the optimal auxiliary slot structure parameters optimized by the third-generation genetic algorithm, the prototype motor is brought in and the optimized IPMSM finite element simulation is carried out to extract the air gap flux density under rated conditions, calculate the EMF and perform Fourier decomposition. The optimized motor model is shown in Fig. 7. and the spatial-temporal order of the electromagnetic force is shown in Fig. 8.

The radial EMF densities for each order of time at spatial order 0 are shown in Table 6.The comparison of EMF density, average torque, torque ripple and efficiency before and after optimization of time 24 order and 48 order under space 0 order is shown in Table 7. and Table 8.

Table 6. Optimized radial EMF density for each time order at spatial order 0

Time order	Radial EMF density/N/m^2	Time order	Radial EMF density/N/m^2
0	240744.4	40	175.8
8	150.6	48	7698.5
16	193.9	56	215.0
24	9347.5	64	378.7
32	597.1	72	2413.5

Table 7. Comparison of spatial 0th-order time 24th-order and 48th-order EMF density before and after optimization

	F_{r0_24} / N / m^2	F_{r0_48} / N / m^2
Before slotting	14199.2	17818.96
After slotting	9347.5	7698.5
Optimization effect	34.2%↑	56.8%↑

Table 8. Comparison of electromagnetic performance before and after optimization

	Average torque/N*m	Torque ripple	Efficiency
Before slotting	297.96	26.32%	95.03%
After slotting	295.11	13.24%	95.13%
Optimization effect	0.96%	49.7%↑	0.11%↑

From Table 7, it can be seen that the motor, under rated working condition, the spatial-0th order time-24th order EMF density decreases from 14199.2 to 9347.5 N/m^2 after slotting, optimization results in a 34.2% improvement compared to the prototype motor, and the spatial 0th order time 48th order EMF density decreases from 17818.9 to 7698.5 N/m^2 , optimization results in a 56.8% improvement compared to the prototype motor. According to the results, it can be seen that optimization effect is obvious. From Table 8, it can be seen that the optimized motor torque decreases from 297.96 to 295.11 N*m, the torque pulsation is reduced from 15.32% to 13.24% and the efficiency increased to 95.13%. Most importantly, the comprehensive E-NVH performance has been improved by 45.14%. According to the analysis of the optimized results, it can be seen that after the optimization of the rotor auxiliary slot parameters, the main EMF order that causes electromagnetic vibration of the 8-pole 48-slot motor is greatly reduced, and although the torque of the motor decreases, the magnitude of the decrease is very small, and the optimized motor torque meets the performance requirements, and at the same time, the torque ripple of the motor is also weakened, and the motor efficiency is improved. In summary, the optimization method based on NSGA-Ⅲ used in this paper to optimize the parameters of the rotor auxiliary slots directly

with the optimization objective of reducing the EMF of a specific order is effective.

4 Conclusion

In this paper, an innovative E-NVH comprehensive performance optimization method for IPMSM is constructed by establishing rotor auxiliary slots to target weakening harmonic electromagnetic force. The proposed NSGA-III-based co-optimization strategy breaks through the traditional design paradigm of taking the torque performance as a single target, and achieves a global balance of the comprehensive motor performance in terms of harmonic electromagnetic force, average torque, torque pulsation, and efficiency. The research confirms that the comprehensive E-NVH performance of IPMSM can be significantly improved by targeting the intervention of specific harmonic order EMF.

5 References

[1] L. Zhu et al., "Design, Optimization, and Experimental Study of a Novel Direct-Driven Linear-Rotary Wave Generator," in IEEE Transactions on Energy Conversion,2025.

[2] Q. Li, S. Liu, W. Fang, X. Li and Z. Tse, "Sideband Vibration Suppression of Interior Permanent Magnet Synchronous Motors for Electric Vehicles Under Multiple Operating Conditions," in IEEE Transactions on Transportation Electrification, vol. 9, no. 1, pp. 322-335, March 2023.

[3] J. Ma and Z. Q. Zhu, "Mitigation of Unbalanced Magnetic Force in a PM Machine With Asymmetric Winding by Inserting Auxiliary Slots," in IEEE Transactions on Industry Applications, vol. 54, no. 5, pp. 4133-4146, Sept.-Oct. 2018.

[4] Q. Li, S. Liu and Y. Hu, "Vibration Characteristics of Permanent Magnet Motor Stator System Based on Vibro-Inertance Matrix Method," in IEEE Transactions on Energy Conversion, vol. 37, no. 3, pp. 1777-1788, Sept. 2022.

[5] M. Xu, W. Zhao, J. Ji, Q. Chen and G. Liu, "Auxiliary Notching Rotor Design to Minimize Torque Ripple for Interior Permanent Magnet Machines," in IEEE Transactions on Industrial Electronics, vol. 71, no. 10, pp. 12051-12062, Oct. 2024.

[6] S. Wang, X. Zhang, X. Zhao, S. Niu and W. Fu, "A Novel Slot-PM Assisted Complementary-Rotor Doubly Salient Machine With Enhanced Torque Performance," in IEEE Transactions on Industrial Electronics, vol. 69, no. 11, pp. 11499-11509, Nov. 2022.

[7] X. Zhao and S. Niu, "Design and Optimization of a Novel Slot-PM-Assisted Variable Flux Reluctance Generator for Hybrid Electric Vehicles," in IEEE Transactions on Energy Conversion, vol. 33, no. 4, pp. 2102-2111, Dec. 2018.

[8] D. Li, Y. Xie, W. Cai and F. Zhang, "Vibration Mitigation of Interior Permanent Magnet Synchronous Motor Using a Targeted Rotor-Step Skewing Method," in IEEE Transactions on Transportation Electrification, vol. 11, no. 1, pp. 2160-2170, Feb. 2025.

[9] D. Li, Y. Xie, W. Cai, F. Zhang and Y. Sun, "An Analytical Prediction Method for Zero-Order Vibration and Noise of Permanent Magnet Synchronous Motor," in IEEE Transactions on Applied Superconductivity, vol. 34, no. 8, pp. 1-6, Nov. 2024.

[10] Q. Li, S. Liu, X. Li and Y. Hu, "Vibro-Inertance Matrix Supported OCF Characteristics Analysis of PMSM Under Multiple Operating Conditions for EV," in IEEE Transactions on Industrial Electronics, vol. 71, no. 1, pp. 126-137, Jan. 2024.

[11] C. Peng, D. Wang, B. Wang, J. Li, C. Wang and X. Wang, "Different Rotor Segmented Approaches for Electromagnetic Vibration and Acoustic Noise Mitigation in Permanent Magnet Drive Motor: A Comparative Study," in IEEE Transactions on Industrial Electronics, vol. 71, no. 2, pp. 1223-1233, Feb. 2024.

[12] C. Liu, S. Zuo, X. Wu, B. Yin, H. Zhuang and S. Wang, "Torque Ripple Reduction of Permanent Magnet-Assisted Synchronous Reluctance Motors Based on Equivalent Slotting Effect and Auxiliary Flux Barriers," in IEEE Transactions on Transportation Electrification, vol. 11, no. 2, pp. 7054-7065, April 2025.